JOURNAL OF MATERIALS SCIENCE 33 (1998) 4609–4620

Dielectric and structural properties of A-cation-deficient perovskites, tetragonal tungsten bronzes and their composites in the $K_2Sr_4(Mg_xNb_{10-x})Li_{3x}O_{30}$ system

B. TRIBOTTE, M. HERVIEU, G. DESGARDIN
Laboratoire CRISMAT/ISMRA, (CNRS-UMR 6508), 6 bd Maréchal Juin, 14050 CAEN Cedex, France

In the $K_2Sr_4(Mg_xNb_{10-x})Li_{3x}O_{30}$ system ($0 \leqslant x \leqslant 1.33$), two phases, one having a tetragonal tungsten bronze (TTB) structure and the other having a perovskite-type structure, are observed after calcination and sintering. The synthesis of single-phase samples, having either of these structure types, has allowed for the determination of their respective contribution to the system's dielectric properties, specifically $\varepsilon_r' = f(T)$ and $tg\delta = f(T)$ over the temperature range -60 to $150\,^{\circ}C$. Using X-ray and electron diffraction techniques, scanning electron microscope observations and energy dispersive spectroscopy analysis, various A-cation-deficient perovskite phases were characterized, in particular $Sr_{0.8}(Mg_{0.2}Nb_{0.8})O_3$. The compositional ability of the TTB structure in this system is also correlated to the $\varepsilon_r' = f(T)$ curves, which exhibit a broad maximum.

1. Introduction

Recent investigations have shown that composite ceramics consisting of phases that adopt the tetragonal tungsten bronze structure (TTB) and the perovskite structure, such as mixing $K_2Sr_4Nb_{10}O_{30}$ (KSN) with $Pb(Mg_{1/3}Nb_{2/3})O_3$ (PMN), are of interest in obtaining dielectric properties exhibiting flat $\varepsilon_r' = f(T)$ curves [1, 2]. The choice in mixing these structural types was in part driven by the close relationship of the TTB structure (Fig. 1) to that of the perovskite, since the octahedral framework of the former leads to, beside pentagonal and trigonal tunnels, tetragonal tunnels similar to the perovskite cages [3]. As described previously [4], mixing of oxides that adopt these two structures has led to solid solutions and induced dielectric curves with a flat temperature profile. This was attributed to partial diffusion of the cations between the different sites of the closely related structures. We have, therefore, undertaken a study to discern the respective contribution of these phases to the dielectric properties. We have chosen a TTB family, which allows for a wide range of compositional variation, as described by Scott *et al.* [5] in the $KNbO_3$–$SrNb_2O_6$ system. The TTB structure can also accommodate cationic substitutions; in particular, magnesium, which has been observed to occupy the octahedral sites of niobium-based perovskites [6], is thought to prefer the niobium sites in $K_2Sr_4Nb_{10}O_{30}$.

In order to maintain full occupancy of the tetragonal and pentagonal tunnels, by K^+ and Sr^{2+}, when the substitution of Mg^{2+} for Nb^{5+} was made, a cosubstitution that can charge-balance the prior substitution is required. With this aim, we attempted to introduce the small Li^+ cation in the empty trigonal tunnels of the TTB structure.

Different compositions were therefore investigated, according to the chemical formula $K_2Sr_4(Nb_{10-x}Mg_x)Li_{3x}O_{30}$ with $0 \leqslant Li^+ \leqslant 4$ or $0 \leqslant x \leqslant 1.33$. The X-ray diffraction of calcined powders and the dielectric properties of sintered samples in this system have already been reported [7]. It was shown that two phases, one with the TTB structure and the other with the perovskite structure, are present after the calcination and sintering process. The perovskite is present as a majority phase for $x \geqslant 1$. An isotype of perovskite was also observed for the composition $Sr_6(Mg_2Nb_8)Li_4O_{30}$.

The present work concerns a transmission electron microscopy study of the (K, Sr) (Mg, Nb) Li, O system including energy dispersive spectroscopy (EDX) analysis, to determine the composition of the bronze and perovskite phases. These results led to investigation of the Sr (Mg, Nb) O system and to the synthesis of A-cation-deficient perovskites $Sr_{0.8}(Mg_{0.2}Nb_{0.8})O_3$ and $Sr_{0.875}(Mg_{0.25}Nb_{0.75})O_3$. Finally, we investigated different compositions to realize both the TTB and the perovskite as pure samples, to elucidate their respective contributions to the dielectric properties.

2. Experimental procedure

2.1. Synthesis

The different compositions in the (K, Sr, Mg, Nb, Li) O system were synthesized from Nb_2O_5 (99.9% purity, H.C. Starck) and K_2CO_3, $SrCO_3$, Li_2CO_3 (99% purity, Prolabo) and MgO (96% purity, Prolabo). The reagent mixture was wet-attrition milled in ethanol.

The calcination was performed using a standard thermal cycle for the synthesis of $K_2Sr_4Nb_{10}O_{30}$, i.e. heating in air at 1200 °C for 4 h with a heating–cooling rate of 150 °C h^{-1}. After calcination, a second attrition milling was carried out to attain a monomodal grain size distribution. The sintering of pressed samples (100 MPa) was performed at 1100, 1200 or 1300 °C with a dwell time of 2 h (heating–cooling rate of 150 °C h^{-1}).

2.2. Characterization of the ceramics

The calcined powders and the sintered ceramics were characterized by X-ray diffraction (XRD) using either a Guinier camera or a diffractometer, both using Cu$K_{\alpha 1}$ radiation. Structure refinement and pattern matching were made with the Fullprof program [8] (Rietveld method). Specimens for transmission electron microscopy were prepared from ground sintered discs. The crystallites were deposited on a holey carbon grid. The electron diffraction investigation was carried out using a Jeol 200CX, equipped with a tilting rotating sample holder ($\pm$ 60°) and an EDX detector (Kevex). The microstructures were studied by scanning electron microscopy (SEM), using a Jeol JSM 840 or a Philips XL30 FEG, equipped with EDX detectors, respectively a Tracor 5500 or an Oxford Link Isis 300. EDX analysis (using standards as references) can only provide information on the K, Sr, Mg and Nb contents (not Li nor O). The cation ratios given for the different compounds herein correspond to the average analyses, which were performed on several grains. Thus, in deducing our compositions, the lithium content is calculated using the assumption of a fully occupied oxygen sublattice in the perovskite and TTB phases, corresponding to formula in O_3 or O_{30}. The dielectric measurements were performed using a Hewlett-Packard 4262A RLC bridge at 1 kHz. The sintered discs, whose faces were painted with an In–Ga alloy to make a capacitor, were placed in a Weiss Technik chamber, which could be regulated between $-$ 60 and 150 °C. The resistance measurements were made with a direct current (d.c.) bias field equal to 63 V (Sefelec bridge CS1010A).

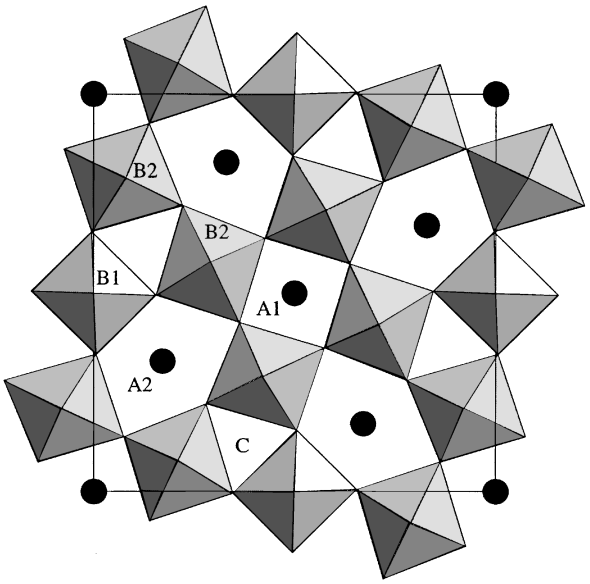

Figure 1 Tetragonal tungsten bronze structure of $(Al)_2(A2)_4C_4(B1)_2(B2)_8O_{30}$ projected onto the (0 0 1) plane, with the B1 and B2 octahedral sites and the A1 tetragonal, A2 pentagonal and C trigonal tunnels.

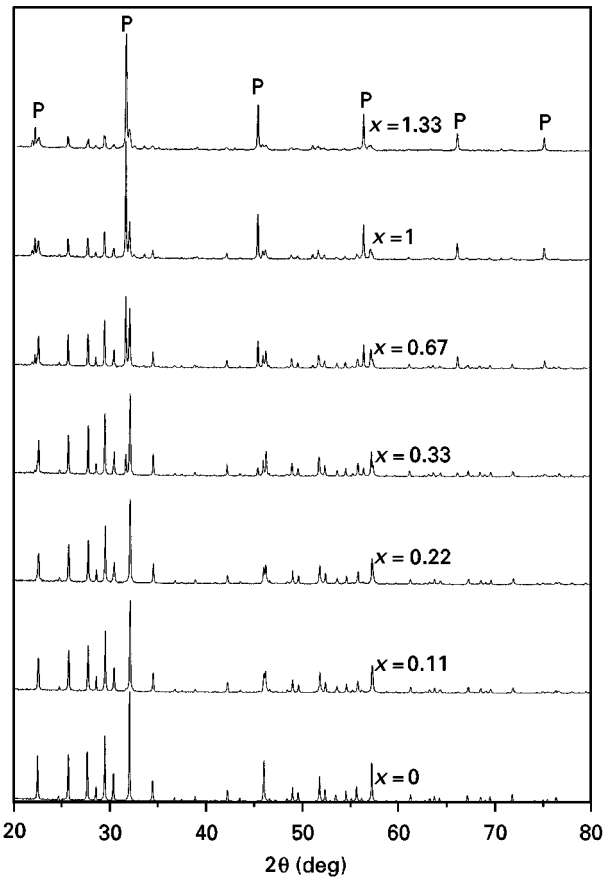

Figure 2 XRD patterns of powders, calcined at 1200 °C for 4 h, having the nominal compositions $K_2Sr_4(Mg_xNb_{10-x})Li_{3x}O_{30}$.

3. Results and discussion

3.1. Preliminary results in the $K_2Sr_4(Mg_xNb_{10-x})Li_{3x}O_{30}$ system with $0 < x \leqslant 1.33$

As seen previously for this system [7], two phases, a tetragonal tungsten bronze (structure given in Fig. 1) and a perovskite, are present after calcination and sintering. The diffractograms for several compositions are given in Fig. 2, and the perovskite phase, which is dominant for $x \geqslant 1$, does not correspond to any known perovskite (such as $KNbO_3$, $Li_{0.25}SrNb_{0.75}O_3$ or $Sr(Mg_{1/3}Nb_{2/3})O_3$).

Cell parameter refinements from XRD data of both the perovskite and TTB phases reveal a constant cell parameter, a_P, for the perovskite, regardless of the

TABLE 1 Cell parameters of the perovskite and TTB phases present after calcination at 1200 °C for 4 h, for the nominal compositions $K_2Sr_4(Mg_xNb_{10-x})Li_{3x}O_{30}$

Nominal compositions	a_P(nm)[a]	a_{TTB}(nm)[b]	c_{TTB}(nm)[b]	$a_{TTB}/(a_{TTB}/c_{TTB}\cdot\sqrt{10})$
$K_2Sr_4Mg_{0.11}Nb_{9.89}Li_{0.33}O_{30}$	–	1.2464	0.3930	1.0029
$K_2Sr_4Mg_{0.22}Nb_{9.78}Li_{0.67}O_{30}$	–	1.2474	0.3925	1.0050
$K_2Sr_4Mg_{0.33}Nb_{9.67}Li_1O_{30}$	0.3993	1.2481	0.3923	1.0060
$K_2Sr_4Mg_{0.67}Nb_{9.33}Li_2O_{30}$	0.3993	1.2495	0.3927	1.0062
$K_2Sr_4Mg_1Nb_9Li_3O_{30}$	0.3994	–	–	–
$K_2Sr_4Mg_{1.33}Nb_{8.67}Li_4O_{30}$	0.3995	–	–	–

[a]P, perovskite-type phase.
[b]TTB, tetragonal tungsten bronze phase.

overall composition. On the contrary, the cell parameters of the TTB phase, a_{TTB} and c_{TTB}, follow a notable evolution with composition (Table I). This seems to indicate that there is a defined composition for the perovskite phase, whereas for the TTB phase there exists wide range of solid solution behaviour.

SEM observations were made on polished, thermally etched (to reveal the grain boundaries), sintered discs. As seen in Fig. 3, different contrasts were observed and were associated with different compositions by EDX analysis. Some of them contained only Mg and Nb with a ratio of 0.4 : 1, while others contained K, Sr and Nb with compositions varying from 0.2 : 0.3 : 1 to 0.15 : 0.53 : 1.

Regardless of the sintering cycle, either 1200 °C for 2 h, 1200 °C for 8 h or 1300 °C for 2 h (all with a heating and cooling rate of 150 °C h^{-1}), the $\varepsilon_r' = f(T)$ and $tg\delta = f(T)$ curves were very similar. Representative curves from measurements of samples sintered at 1200 °C for 2 h after a calcination at 1200 °C for 4h are shown in Fig. 4, for the nominal compositions $K_2Sr_4(Mg_xNb_{10-x})Li_{3x}O_{30}$ with x varying from 0.11 to 1.33. One can relate the evolution of these curves to the changes in the XRD patterns, i.e. to the nature and amount of the different phases. Overall, the mean level of ε_r' (Fig. 4) decreases significantly as the perovskite amount increases (Fig. 2). Moreover, as x increases, i.e. when the magnesium or lithium content increases, both the maximum temperature and ε_r' decrease, and

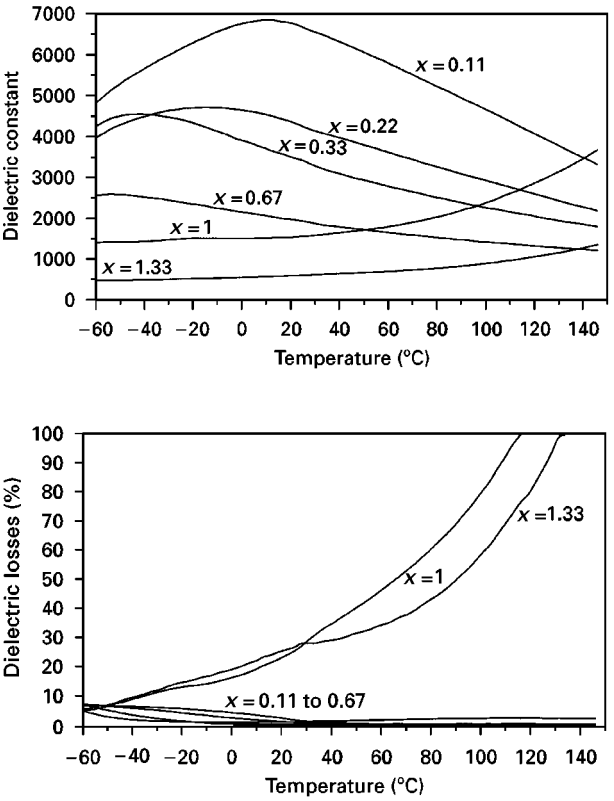

Figure 4 Dielectric constants and losses versus temperature of samples sintered at 1200 °C for 2 h, having the nominal compositions $K_2Sr_4(Mg_xNb_{10-x})\ Li_{3x}O_{30}$.

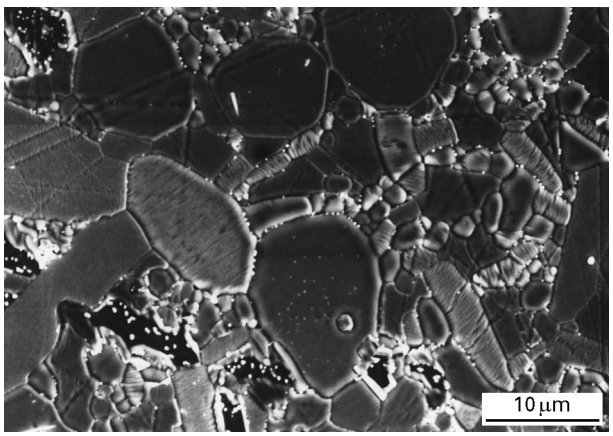

Figure 3 Microstructure of a sample, sintered at 1200 °C for 2 h, having the nominal composition $K_2Sr_4(Mg_{0.67}Nb_{9.33})Li_2O_{30}$.

the transition broadens with respect to temperature. For $x \geqslant 1$, the shape of the curves is different and is characterized by a drastic increase of the dielectric losses with temperature, which causes a significant increase of observed ε_r'. The origin of this evolution can be correlated to the presence of the small, mobile Li^+ cation ($r \approx 0.06$ nm) within the structure. Insulation resistance measurements, carried out on these samples at room temperature, showed that resistivities decreased from $1.5 \times 10^{12}\,\Omega$cm for the lithium poor composition $K_2Sr_4(Mg_{0.33}Nb_{9.67})Li_1O_{30}$ to $2 \times 10^8\,\Omega$cm for the lithium rich one, $K_2Sr_4(Mg_{1.33}Nb_{8.67})Li_4O_{30}$. Thus, in the lithium rich compounds, conduction effects may appear at higher temperatures and contribute to high dielectric losses.

3.2. Electron and X-ray diffraction studies of the perovskite phase in the (K,Sr)(Mg,Nb) Li, O system

The electron diffraction investigation of the sample $K_2Sr_4(Mg_{0.67}Nb_{9.33})Li_2O_{30}$ (composition I) showed that there exists a perovskite-type compound as a secondary phase, along with the TTB structure. Reconstruction of the reciprocal space gave evidence for a single cubic perovskite cell with a_p close to 0.4 nm. A typical [0 0 1] electron diffraction pattern is given in Fig. 5a. However, by tilting systematically about the [0 0 1]* and [1 1 0]* directions, in some crystallites, extra reflections were observed, often in incommensurate positions. An example of a $[\bar{1}\,1\,0]$ pattern is given in Fig. 5b where the satellites are lying along the [1 1 1]*, with $q \approx 0.22\ d_{111}$. These more complex features are attributed to short range order in the octahedral layers of the perovskite. The EDX analysis of the perovskite-type crystallites showed that the average cation ratio, K : Sr : Mg : Nb is close to 1 : 4 : 1 : 6, i.e. to $K_{0.14}Sr_{0.57}(Mg_{0.14}Nb_{0.86})$ calculated for $\sum(Mg + Nb) = 1$. The presence of Li in this phase cannot, however, be detected by EDX. The Mg : Nb ratio of this new perovskite, namely 1 : 6, is significantly higher than the nominal value (1 : 14) of the starting composition.

Referring to the nominal formula $K_2Sr_4(Mg_xNb_{10-x})Li_{3x}O_{30}$, an increase of the Mg content up to $x = 1.33$ is possible by a (K + Sr)/Nb balance, if we consider all four trigonal tunnels occupied by lithium. We have therefore considered the composition $Sr_6(Mg_2Nb_8)Li_4O_{30}$ (composition II), directly deduced from composition I. The calcination led to a nearly pure perovskite, isostructural with the former (in composition I). The few weak lines that are present in the XRD diagram are attributed to phases of the (Nb,Mg) O system, which may or may not include lithium. The SEM analysis also showed the presence of a secondary phase, as shown in Fig. 6 in the form of grains labelled d; EDX indicated that these grains contained only Mg and Nb, in ratio of 0.32 : 1. EDX analysis, when systematically coupled with electron diffraction showed that there exists a non-stoichiometry domain for the A-site cation in the perovskite phase. The measurements carried out on numerous crystallites led to the average cationic composition $Sr_{0.65}(Mg_{0.15}Nb_{0.85})$.

Comparison of the actual cationic (except Li) compositions of the two perovskite phases observed herein, $K_{0.14}Sr_{0.57}(Mg_{0.14}Nb_{0.86})$ and $Sr_{0.65}(Mg_{0.15}Nb_{0.85})$, is interesting because they exhibit the same Mg : Nb ratio (in the limit of accuracy of the technique). They differ only in the type and the content of the cations residing on the twelve-fold co-ordinated A-sites. In facts, about 0.14 K^+ is replaced by 0.08 Sr^{2+}, on going from the first compound to the second, which corresponds to direct compensation of the charge balance. This compensation mechanism can be expressed in the following cationic chemical formula: $K_{2y}Sr_{0.65-y}(Mg_{0.14}Nb_{0.86})$.

To understand the compositional stability of these perovskites, only the heavy cation content was first considered. The effect of the presence of lithium was subsequently taken into consideration. Thus,

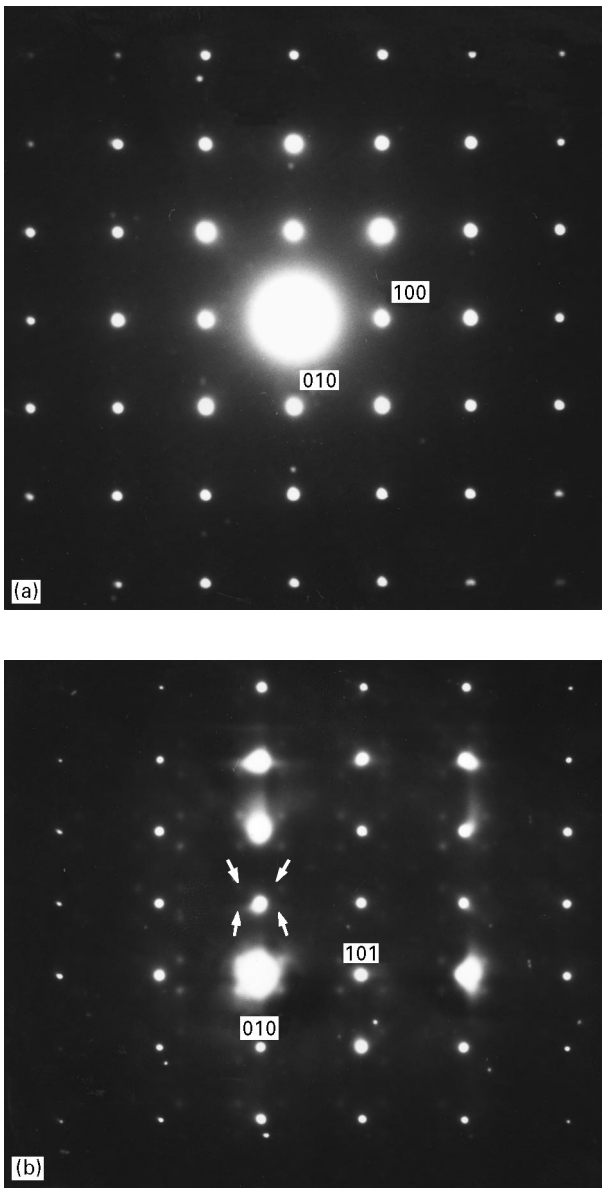

Figure 5 Electron diffraction patterns from (a) the [0 0 1] and (b) the $[\bar{1}\ 1\ 0]$ zone axes of the perovskite-type phase in the compound $K_2Sr_4(Mg_{0.67}Nb_{9.33})Li_2O_{30}$, after sintering at 1200 °C for 2 h.

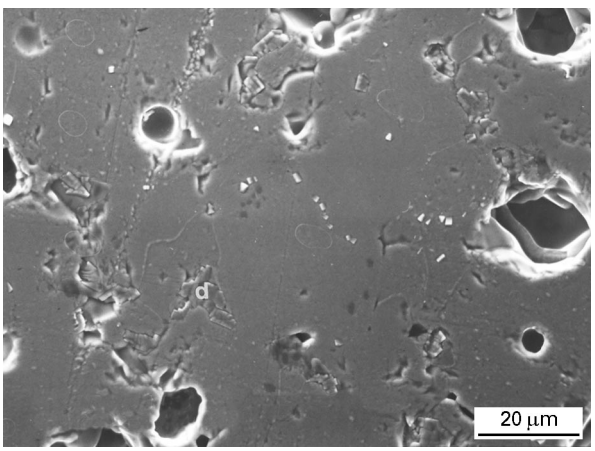

Figure 6 Microstructure of a sample, sintered at 1200 °C for 2 h, having the nominal composition $Sr_6(Mg_2Nb_8)Li_4O_{30}$.

a compound of nominal composition $K_{0.14}Sr_{0.57}(Mg_{0.14}\ Nb_{0.86})$ was synthesized by calcination at 1200 °C for 4 h. The XRD pattern revealed the presence of two phases: a TTB and a cubic perovskite with a cell parameter close to 0.4 nm, similar to that of composition I. The cell parameters of the TTB and the cubic perovskite phases were refined from the XRD data and found to be: $a_{TTB} = 1.246$ nm, $c_{TTB} = 0.392$ nm $[a/(c \cdot 10) = 1.005]$ and $a_p = 0.399$ nm. Polished and thermally etched discs of this composition, which were sintered at 1300 °C for 2 h, were analysed by SEM. Particularly in the back scattered electron mode (Fig. 7), the contrast shows two kinds of grains in the matrix, which are joined with a third set of darker grains, which are minor in content. EDX analysis showed two distinct average compositions. When considering the (Mg + Nb) content as equal to one and therefore the oxygen content as three, consideration of the (K + Sr) content allows each of the average compositions to be correlated with one of the structures observed by XRD. The compositions with $(K + Sr) \leqslant 0.6$ correspond to an $A_{0.6}BO_3$ TTB structure having full or partially occupied A-sites, while the compositions with $0.6 < (K + Sr) \leqslant 1$ correspond to an ABO_3 perovskite-type structure, also with the possibility of vacancies on A-sites. Using these considerations with the EDX results, for the nominal composition $K_{0.14}Sr_{0.57}Mg_{0.14}Nb_{0.86}$, we believe the TTB phase corresponds to the grains observed with the $K_{1.3}Sr_{4.4}(Mg_{0.2}Nb_{9.8})O_{30}$ composition, and the perovskite phase with those of the $K_{0.13}Sr_{0.68}(Mg_{0.17}\ Nb_{0.83})O_3$ composition. Interestingly, the Mg : Nb ratio in the perovskite (0.2) is ten times greater than that in the TTB structure. The third set of darker grains observed in this sample (Fig. 7) contains only Mg and Nb in an unusual ratio of 1.6 : 1, which, to our knowledge, does not correspond to any known compound.

The presence of lithium must be taken into account because it appears to be strongly associated to the formation of the K : Sr based perovskite. Two ideal compositions may be proposed for the mixed perovskite, keeping the K : Sr : Mg : Nb ratio constant and assuming the oxygen sites are fully occupied.

$$[(K_{1/7}Sr_{4/7}Li_{2/7})(Mg_{1/7}Nb_{6/7})]_{3/3.07}O_3$$

which supposes that a very small deficiency (approximately 2%) exists on both the A and B cation sites (composition III) and

$$[(K_{1/7}Sr_{4/7}Li_{1/7})(Mg_{1/7}Nb_{6/7})]O_3$$

which supposes that the B-sites are fully occupied and vacancies reside on 1/7 (approximately 14%) of the A-sites (composition IV).

Both compositions were synthesized following the usual thermal process. The XRD patterns confirmed that the major phase is a perovskite, isotypic with the one observed in composition I. Only traces of TTB are observed in composition IV, whereas secondary phases (called φ_i) are observed for composition III, probably due to an excess of lithium. The cell parameters are 0.3994 and 0.3993 nm, for compositions III and IV, respectively. These parameters are very close to that of the perovskite described in Table I. SEM observations, coupled with EDX analysis, were performed on these two samples, after sintering at 1200 °C for 2 h. A micrograph of sample IV is shown in Fig. 8. The matrix corresponds to a phase having the composition $(K_{0.13}Sr_{0.60}Li_{0.09})\ (Mg_{0.14}Nb_{0.86})\ O_3$ (where the lithium content was deduced from electroneutrality and assuming the oxygen content to be three). The light grains (in the back scattered electron mode) were correlated to the TTB structure present in the XRD diagram and correspond to the formula $(K_{1.78}Sr_{3.68}Li_{1.46})\ (Mg_{0.2}Nb_{9.8})O_{30}$. Some darker grains (Fig. 8) were also observed that contain mainly Mg and Nb. The EDX analysis on the sample of composition III revealed the same cation distribution for the perovskite phase.

In conclusion, considering its near-pure XRD diagram, $(K_{1/7}Sr_{4/7}Li_{1/7})\ (Mg_{1/7}Nb_{6/7})O_3$ seems to be the appropriate composition, leading to the formation of the perovskite observed in the nominal composition $K_2Sr_4(Mg_xNb_{10-x})Li_{3x}O_{30}$ $(0 < x \leqslant 1.33)$. Indeed, we have shown that the same perovskite phase is observed regardless of the composition in this system, contrary to the TTB phase whose parameters vary.

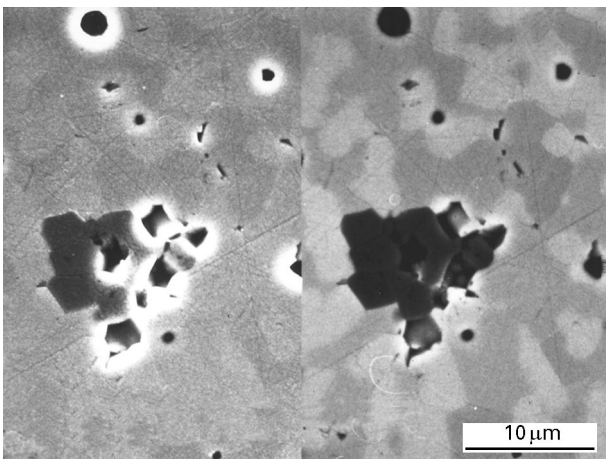

Figure 7 Microstructure of a sample, sintered at 1300 °C for 2 h, having the nominal composition KSr_4MgNb_6 in secondary electron mode (left) and back scattered electron mode (right).

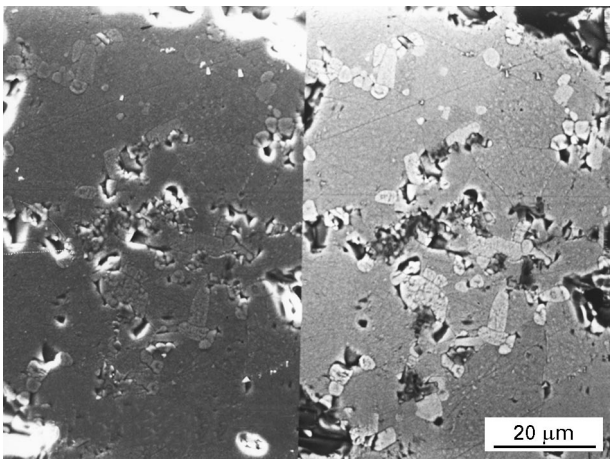

Figure 8 Microstructure of a sample, sintered at 1200 °C for 2 h, having the nominal composition $(K_{1/7}Sr_{4/7}Li_{1/7})\ (Mg_{1/7}Nb_{6/7})O_3$, in secondary electron mode (left) and back scattered electron mode (right).

On the other hand, the perovskite present in the $Sr_6(Mg_2Nb_8)Li_4O_{30}$ compound (II) corresponds to the cation composition $Sr_{0.65}(Mg_{0.15}Nb_{0.85})$, as determined by EDX, ED and SEM observations. It is obvious that lithium is strongly associated to the formation of this perovskite and, in a manner as above, one can expect the formula to be $Sr_{0.65}Li_{0.15}(Mg_{0.15}Nb_{0.85})O_3$ (composition V). This composition was therefore synthesized, using the usual thermal cycle; this yielded a perovskite phase with $a = 0.398$ nm and only traces of a TTB phase.

These results confirm the existence of two perovskites, namely $(K_{0.14}Sr_{0.57}Li_{0.14})(Mg_{0.14}Nb_{0.86})O_3$ and $(Sr_{0.65}Li_{0.15})(Mg_{0.15}Nb_{0.85})O_3$, which have the same Mg : Nb ratio and the latter can be derived from the former by replacing 0.14 K^+ with only 0.07 Sr^{2+}.

3.3. Perovskites in the Sr (Mg, Nb)O_3 system

Both the evidence of an existence range for perovskite of composition II (nominal composition $Sr_6(Mg_2Nb_8)Li_4O_{30}$) and the ability to stabilize Sr-deficient niobates with the perovskite structure led us to investigate the system $Sr_{(1+3x)/2}(Mg_xNb_{1-x})O_3$, between the two limits $x = 0$ and $x = 1/3$. The compound $Sr_{0.5}NbO_3$ ($x = 0$) is an orthorhombic bronze [9] and $Sr(Mg_{1/3}Nb_{2/3})O_3$ ($x = 1/3$) is an hexagonal perovskite with 1–2 order along the [1 1 1] direction of the cubic cell [10]. In order to realize good crystallization and to minimize the formation of secondary phases, seven compositions belonging to this system were synthesized according to the following cycle: 1200 °C for 4 h, with a heating rate of 150 °C h^{-1} and a cooling rate of 5 °C h^{-1} until 1000 °C, then 150 °C h^{-1} cooling rate. The corresponding XRD patterns, after calcination are shown in Fig. 9. Only two compositions, $x = 0.2$ and $x = 0.25$, correspond to single-phase perovskites. Having a nominal composition halfway between the two limits ($x = 0$ and $x = 1/3$), the $Sr_{0.8}(Mg_{0.2}Nb_{0.8})O_3$ compound ($x = 0.2$) has an XRD pattern characteristic of a simple perovskite phase. The structure-refinement (using the Fullprof program) of this perovskite, with $a = 0.398$ nm, was based on the space group Pm3m with atoms at the following locations in the unit cell: Sr : 1/2, 1/2, 1/2 Mg, Nb : 0, 0, 0 and O : 0, 1/2, 0. Refinement of the site occupancies gave the composition $Sr_{0.806}(Mg_{0.204}Nb_{0.796})O_3$ (R-Bragg = 3.48%). EDX analysis performed on a sintered sample (1450 °C for 2 h) using the SEM, gave a similar cationic composition, $Sr_{0.77}(Mg_{0.17}Nb_{0.83})$. The stabilization of this cation-deficient niobate having a perovskite structure, can be compared to that of Sr_xNbO_3 ($x = 0.72$, 0.82 or 0.86), but in the latter niobium exhibits a mixed valence Nb^{4+}/Nb^{5+} [11,12].

In contrast to the $x = 0.20$ compound, the $Sr_{0.875}(Mg_{0.25}Nb_{0.75})O_3$ compound ($x = 0.25$) presents a superstructure typical of an 1–3 ordered perovskite, and distinctly different from the 1–2 ordering of the "hexagonal" perovskite. This phase adopts a cubic or slightly orthorhombic cell, and its structure is presently being investigated by coupled X-ray, neutron diffraction and electron diffraction.

After a further sintering cycle, no changes appear in the XRD patterns of these compositions, except for the $x = 0.25$ compound whose superstructure reflections disappear, implying a random distribution of the cations over their sites of the structure. Concerning the sintering behaviour of these materials, a weak densification was obtained for most of the ceramics after sintering at 1300 °C for 2 h (150 °C h^{-1}) and quite good densification was obtained only after a sintering at 1450 °C for 2 h (150 °C h^{-1}). For example, $Sr_{0.8}(Mg_{0.2}Nb_{0.8})O_3$ sintered in the latter conditions has a relative density of 93% of the theorical density.

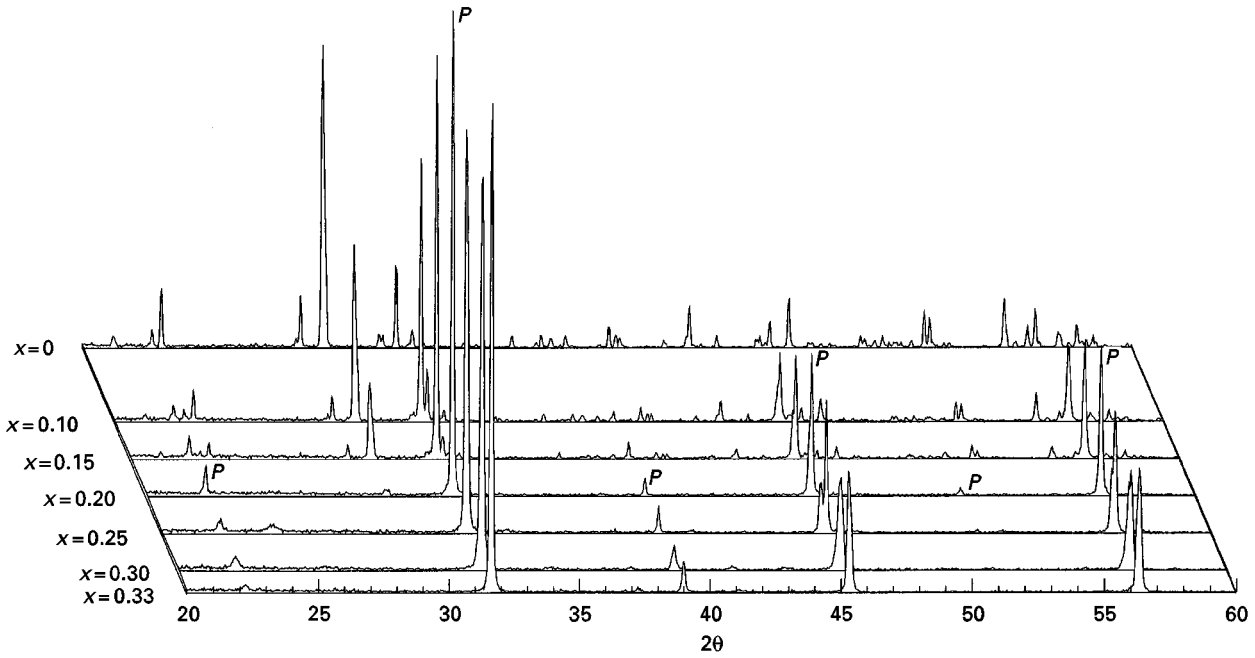

Figure 9 XRD patterns of calcined powders, having $Sr_{(1+3x)/2}(Mg_x\ Nb_{1-x})O_3$ compositions.

3.4. Perovskites in the (K,Sr) (Mg,Nb)O_3 system

The above-mentioned results (cf. Sections 3.2 and 3.3) led us to consider A-cation-deficient perovskites, based on the $Sr_{0.8}(Mg_{0.2}Nb_{0.8})O_3$ or $Sr_{0.875}(Mg_{0.25}Nb_{0.75})O_3$ compounds, by partial substitution of Sr^{2+} by K^+, with the chemical formula $(K_ySr_{0.8-y})(Mg_{0.2-y/3}Nb_{0.8+y/3})O_3$ or $(K_zSr_{0.875-z})(Mg_{0.2-z/3}Nb_{0.75+z/3})O_3$ respectively. In these efforts to stabilize A-cation-deficient perovskite with potassium and without lithium, we investigated the $(K_ySr_{0.8-y})(Mg_{0.2-y/3}Nb_{0.8-y/3})O_3$ system because one of the compositions, i.e. $(K_{0.15}Sr_{0.65})(Mg_{0.15}Nb_{0.85})O_3$ ($y = 0.15$) is very close to that of $K_{0.14}Sr_{0.57}Mg_{0.14}Nb_{0.86}$, which was found from EDX analysis to be the cationic composition of the perovskite in composition I (cf. Section 3.2)

Compositions with $y = 0.10, 0.13, 0.15, 0.17$ and 0.20 were therefore synthesized by calcination at 1200 °C for 4 h (heating–cooling rate of 150 °C h^{-1}).

Whatever the y value, the XRD patterns showed the formation of two phases: a TTB in small amount and the same perovskite in larger amount. Different thermal cycles were used to determine the appropriate conditions for the formation of the single-phase perovskite. Regardless of the thermal cycle, after various synthetic attempts between 700 and 1200 °C, we were not able to isolate a single-phase perovskite. On the other hand, calcination at high temperature (1200 °C) led to a slight distortion of the octahedra of the TTB cell $[a/(c\cdot\sqrt{10}) \neq 1]$, evidenced by the splitting of the 6 2 0–0 0 2 reflections, which can be mainly attributed to the partial substitution of Nb^{5+} by Mg^{2+}. This splitting reduced as y increased, i.e. when the Mg content decreased.

The XRD diagram of the composition $y = 0.15$, calcined at 1200 °C for 4 h, allowed the determination of the structural parameters of both phases: $a = 0.399$ nm for the perovskite and $a = 1.246$ nm and $c = 0.392$ nm $[a/(c\cdot\sqrt{10}) = 1.005]$ for the TTB phase.

In contrast to the samples sintered at 1200 °C for 2 h, whose splitting of the 6 2 0–0 0 2 reflections decreases as y increases, the samples sintered at 1300 °C for 2 h showed no evolution of the a/c ratio. SEM analysis, coupled with EDX, on these 1300 °C-sintered samples, allowed discrimination between the two types of grains, having two different compositions. Each of these distinct grains can be correlated to either the perovskite or TTB structures. EDX cation compositions are given in Table II as they were calculated to have (Mg + Nb) = 10 or one and assuming an oxygen stoichiometry of O_{30} or O_3 respectively. A constant Mg : Nb ratio is observed in each phase, whatever the y value is, and this is in agreement with the absence of any evolution with y of the XRD diagrams for the TTB phase. It is, in fact, the K : Sr ratio, which is observed to change with the y value, following the K : Sr distribution imposed by the nominal compositions. For all compositions, the TTB phases exhibit a full A-site occupancy with (K + Sr) ≈ 6, whereas the perovskite phases are A-sites deficient with (K + Sr) ≈ 0.8. It should be noted that the Mg : Nb ratio is equal to 0.04 for the TTB, in contrast to 0.2 for the perovskite.

As a conclusion, the synthesis of a single-phase pervoskite in the $(K_ySr_{0.8-y})(Mg_{0.2-y/3}Nb_{0.8+y/3})O_3$ system was not possible following our thermal process. Above 1000 °C, both the perovskite and the TTB phases coexist, and at higher temperatures the magnesium assuredly enters the TTB structure. The occupancy limit of Mg on the octohedral sites in the TTB structure seems to be approximately 0.4. From these results, it appears that a range of Mg compositions may exist for the TTB structure, as well as in the A-cation-deficient perovskite.

3.5. Electron and X-ray diffraction studies of the TTB phase in the (K,Sr) (Mg,Nb) Li,O system

To characterize these complex systems further, a study of the TTB phase present in the nominal compositions $K_2Sr_4(Mg_xNb_{10-x})Li_{3x}O_{30}$ was performed using electron diffraction coupled with EDX analysis.

For the nominal composition I, $K_2Sr_4(Mg_{0.67}Nb_{9.33})Li_2O_{30}$ ($x = 0.67$), a mixture of perovskite and TTB phases is obtained (XRD diagram in Fig. 2). EDX analyses show that there exists a domain of non-stoichiometry for the TTB phase around the average composition of $K_{1.5}Sr_4(Mg_{0.5}Nb_{9.5})$. Note that, for such a composition, a lithium content corresponding to two Li per formula unit would be necessary to keep the oxygen content at 30, leading to the compositional formula $K_{1.5}Sr_4(Mg_{0.5}Nb_{9.5})Li_2O_{30}$. A rather important deviation of the actual cation contents can be observed with regard to the average values, suggesting wide compositional range of the TTB phase. The limits of cationic contents are: $1.3 \leqslant K \leqslant 1.7$, $3.7 \leqslant Sr \leqslant 5.2$, $0.2 \leqslant Mg \leqslant 1.2$ and $8.7 \leqslant Nb \leqslant 9.8$; in a general way, the Sr content increases with the Mg^{2+} substitution for Nb^{5+}. The reconstruction of the reciprocal space and tilting about the a^* and c^* axes allowed for the confirmation of the cell parameters. A typical [0 0 1] ED pattern is

TABLE II EDX compositions of the perovskite and TTB phases present after sintering at 1300 °C for 2 h, for the nominal compositions $K_ySr_{0.8-y}(Mg_{0.2-y/3}Nb_{0.8+y/3})O_3$ ($0.10 \leqslant y < 0.20$)

y	Nominal compositions	TTB phase	Perovskite phase
0.10	$K_{0.10}Sr_{0.70}(Mg_{0.17}Nb_{0.83})O_3$	$K_{1.0}Sr_{5.0}(Mg_{0.4}Nb_{9.6})$	$K_{0.09}Sr_{0.72}(Mg_{0.17}Nb_{0.83})$
0.13	$K_{0.13}Sr_{0.67}(Mg_{0.16}Nb_{0.84})O_3$	$K_{1.2}Sr_{4.7}(Mg_{0.3}Nb_{9.7})$	$K_{0.12}Sr_{0.69}(Mg_{0.17}Nb_{0.83})$
0.15	$K_{0.15}Sr_{0.65}(Mg_{0.15}Nb_{0.85})O_3$	$K_{1.4}Sr_{4.4}(Mg_{0.3}Nb_{9.7})$	$K_{0.14}Sr_{0.68}(Mg_{0.17}Nb_{0.83})$
0.17	$K_{0.17}Sr_{0.63}(Mg_{0.14}Nb_{0.86})O_3$	$K_{1.5}Sr_{4.5}(Mg_{0.4}Nb_{9.6})$	$K_{0.16}Sr_{0.64}(Mg_{0.15}Nb_{0.85})$
0.20	$K_{0.20}Sr_{0.60}(Mg_{0.13}Nb_{0.87})O_3$	$K_{1.5}Sr_{4.5}(Mg_{0.4}Nb_{9.6})$	$K_{0.18}Sr_{0.64}(Mg_{0.16}Nb_{0.84})$

given in Fig. 10a. However, in some areas extra reflections were often observed. One example is shown in Fig. 10b, where the additional spots are indicated by small white arrows. The satellites lie in commensurate positions, which involve a superstructure with a tripling of the a axis and a quadrupling of the d_{021} distance. These patterns attest that complex structural features occur in the bronze matrix, probably correlated with ordering phenomena. Further studies on these phenomena are in progress.

Different compositions belonging to the EDX-determined compositional range were synthesized: $K_{1.5}Sr_4$ $(Mg_{0.5}Nb_{9.5})Li_2O_{30}$ (labelled A), $K_{1.3}Sr_{3.7}$ $(Mg_{0.4}Nb_{9.6})Li_{2.5}O_{30}$ (labelled B) and $K_{1.3}Sr_{3.7}$ $(Mg_{0.33}Nb_{9.67})Li_{2.29}O_{30}$ (labelled C). After different soak times at, and quenching from, 1100 °C, the XRD patterns show a major TTB phase, but secondary phases are also present. Expect for the composition A where a perovskite phase appears along with TTB, identification of the other minor phases, noted φ_i, was difficult because of the numerous niobate-based phases that may exist in this system and the lack of well-indexed phases, especially those including lithium. However, after a calcination at 1200 °C for 4 h, we obtained a nearly single-phase TTB, determined from XRD, for the three compositions A, B and C, and the XRD refinements lead to the cell parameters, which are listed in Table III. This confirms the ability of the TTB phase to accommodate various cationic distributions either by substitutions in the pentagonal and tetragonal tunnels or on the octahedral sites, and also by insertion into the trigonal tunnels (especially by Li^+).

In order to understand the basis of the structural changes, different compositions were prepared as described below.

We investigated first the substitution of Mg^{2+} for Nb^{5+} in $K_2Sr_4Nb_{10}O_{30}$; the resulting charge balance requires a new K^+–Sr^{2+} distribution to maintain full occupancy of the A-site in the TTB structure (Fig. 1). This corresponds to the composition $(K_{2-3x}Sr_{4+3x})$ $(Mg_xNb_{10-x})O_{30}$, which were synthesized for various x values and labelled D for $x = 0.11$, E for $x = 0.13$, F for $x = 0.17$, G for $x = 0.22$ and H for $x = 0.33$.

We also investigated magnesium free compositions having lithium and only partial occupancy of the A-sites in the TTB structure: $K_1Sr_{3.5}Nb_{10}Li_2O_{30}$ (labelled J) and $K_{1.5}Sr_{3.5}Nb_{1.0}Li_{1.5}O_{30}$ (labelled K).

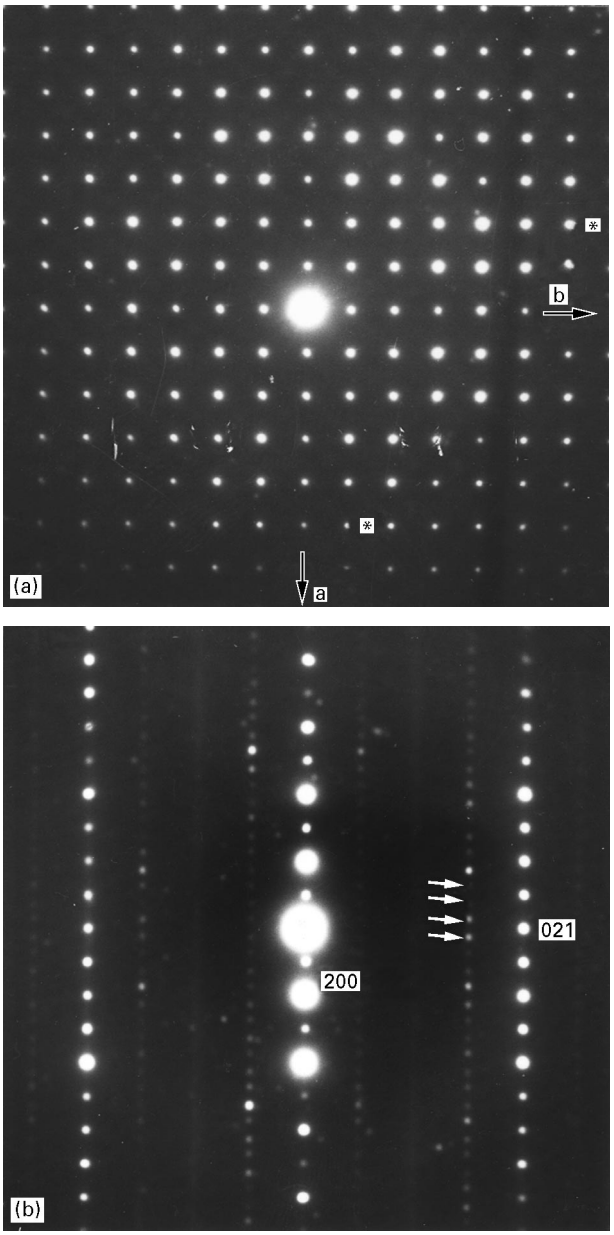

Figure 10 Electron diffraction patterns from (a) the [0 0 1] and (b) the [0 $\bar{1}$ 2] zone axes of the TTB phase, in the compound $K_2Sr_4(Mg_{0.67}Nb_{9.33})Li_2O_{30}$, after sintering at 1200 °C for 2 h.

After calcination at 1200 °C for 4 h, powder XRD patterns showed a single TTB phase for samples D–H,

TABLE III Cell parameters for various compositions of powders, after calcination at 1200 °C for 4 h

	Nominal compositions	a_{TTB} (nm)[a]	c_{TTB} (nm)	$a/(c\cdot\sqrt{10})$	volume (nm^3)	Phase(s)[a,b]
A	$K_{1.5}Sr_4Mg_{0.5}Nb_{9.5}Li_2O_{30}$	1.2485	0.3922	1.0066	0.6113	TTB + P + $\varphi_{2.3}$
B	$K_{1.3}Sr_{3.7}Mg_{0.4}Nb_{9.6}Li_{2.5}O_{30}$	1.247	0.3917	1.0069	0.6093	TTB + $\varphi_{1.23}$
C	$K_{1.3}Sr_{3.7}Mg_{0.33}Nb_{9.67}Li_{2.29}O_{30}$	1.247	0.3918	1.0066	0.6094	TTB + $\varphi_{1.2}$
D	$K_{1.67}Sr_{4.33}Mg_{0.11}Nb_{9.89}O_{30}$	1.247	0.3934	1.0024	0.6117	TTB
E	$K_{1.61}Sr_{4.39}Mg_{0.13}Nb_{9.87}O_{30}$	1.246	0.3930	1.0029	0.6105	TTB
F	$K_{1.49}Sr_{4.51}Mg_{0.17}Nb_{9.83}O_{30}$	1.246	0.3927	1.0037	0.6101	TTB
G	$K_{1.34}Sr_{4.66}Mg_{0.22}Nb_{9.78}O_{30}$	1.245	0.3921	1.0048	0.6086	TTB
H	$K_1Sr_5Mg_{0.33}Nb_{9.67}O_{30}$	1.245	0.3917	1.0058	0.6079	TTB
J	$K_1Sr_{3.5}Nb_{10}Li_2O_{30}$	1.240	0.3904	1.0050	0.6020	TTB + φ_1
K	$K_{1.5}Sr_{3.5}Nb_{10}Li_{1.5}O_{30}$	1.243	0.3916	1.0040	0.6053	TTB + φ_1(+ φ_2)

[a] TTB, tetragonal tungsten bronze phase.
[b] P, perovskite-type and $\varphi_{1,2,3}$ secondary phases.

but a mixture of phases (majority TTB phase with minor phases noted as φ_i) for samples J and K. XRD refinements led to the cell parameters listed in Table III. The $a_{TTB}/(c_{TTB}\cdot 10)$ ratio is an indication of the distortion of the octahedra. As the substitution is increased, the a parameter increases whereas the c parameter decreases to maintain satisfactory interatomic distances. The compositions D–H correspond to a Mg^{2+} for Nb^{5+} substitution, which, as discussed above, implies a change of the $K^+:Sr^{2+}$ ratio. The $a/(c\cdot 10^{1/2})$ ratio increases with Mg content, while both the a and c parameters decrease, for samples D–H. The cell distortion can be understood by substitution of Nb^{5+} ($r \approx 0.064$ nm) by the larger Mg^{2+} ($r \approx 0.072$ nm) on the octahedral sites. At the same time, the decrease of the volume of the cell can be explained by the substitution of K^+($r \approx 0.160$ nm) by the smaller Sr^{2+} ($r \approx 0.144$ nm). The unit cells of the J and K samples present an $a/(c\cdot 10^{1/2})$ ratio different from one and have relatively small volumes (compared with the other ones). All octahedral sites are occupied by Nb^{5+}, so the small cell parameters and the distortion of the octahedra could be explained by either the presence of vacancies or lithium on the A-sites. Lithium may also reside in the trigonal tunnels, as it can adopt different co-ordinations in the TTB structure; a particular example of this concerns the ferroelectric tungsten bronze-type crystal studied by Abrahams *et al.* [13]: $K_{(6-x-y)}Li_{(4+x)}Nb_{(10+y)}O_{30}$ with $x \approx 0.07$ and $y \approx 0.23$. For the general formula $(Al)_2(A2)_4C_4(B1)_2(B2)_8O_{30}$ (Fig. 1), their structure refinement showed the A1 site to be occupied by 87% K and 13% Li, the A2 site by 99% K and 1% Li, the C site by 94% Li and 6% Nb and B-sites fully occupied by Nb.

EDX analyses with SEM were carried out on sintered samples (at 1200 °C for 2 h) of the compositions J and K. The average composition for the TTB phase of sample J was $K_{1.09}Sr_{3.51}Li_{1.89}Nb_{10}O_{30}$, which is very close to the nominal composition and confirms the presence of vacancies on the A and C sites (Fig. 1). In contrast, the EDX analysis of sample K revealed a wide range of compositions, i.e. $1.69 \leqslant K \leqslant 2.30$ and $2.98 \leqslant Sr \leqslant 3.37$ with reference to a $Nb_{10}O_{30}$ formula.

Thus, we can conclude that the A, B and C cells exhibit a strong distortion. The B and C compositions are very close, while the A composition tends to a slightly larger cell. EDX analyses with SEM were performed on sintered samples (at 1200 °C for 2 h), and led to the average compositions of $K_{1.52}Sr_{3.89}Li_{1.21}(Mg_{0.17}Nb_{9.83})O_{30}$ for A, $K_{1.69}Sr_{3.91}Li_{1.06}(Mg_{0.19}Nb_{9.81})O_{30}$ for B and $K_{1.50}Sr_{3.82}Li_{1.37}(Mg_{0.17}Nb_{9.83})O_{30}$ for C. Although the nominal Mg content is different in these three cases ($0.33 \leqslant Mg \leqslant 0.5$), a constant actual Mg content is found, certainly correlated to the common distortion. In comparison to the nominal compositions of the TTB phases, the difference in the Mg content and in the K:Sr ratio, and the presence of lithium may be correlated to the formation of different secondary phases.

3.6. Secondary phases associated with the TTB and perovskite phases

Three phases, labelled φ_1, φ_2 and φ_3, are formed depending on the nominal composition (Table III). The weak intensities and the few reflections did not allow one to identify the different φ_i phases using the ICDD powder diffraction file. However, their presence seems closely related to some evolutions observed in the dielectric properties.

The φ_1, φ_2 and φ_3 phases are associated with TTB formation (Table III) but φ_3 is also present, in addition to the perovskite phases, in the nominal compositions $[(K_{1/7}Sr_{4/7}Li_{2/7})(Mg_{1/7}Nb_{6/7})]_{3/3.07}O_{30}$ (III) and $Sr_6(Mg_2Nb_8)Li_4O_{30}$ (IV). Minor amounts of this phase also appear in the compositions $K_2Sr_4(Mg_xNb_{10-x})Li_{3x}O_{30}$, for the higher values of x ($x = 1$ and 1.33). The φ_i phases appear only when lithium is present in the nominal composition, and φ_3 seems to appear only when the substitution of Nb^{5+} by Mg^{2+} on the octahedral sites of the TTB is realized.

3.7. Dielectric properties of the ceramics in the (K, Sr) (Mg, Nb)Li, O system

The results concerning the $K_2Sr_4(Mg_xNb_{10-x})Li_{3x}O_{30}$ compounds (cf. Section 3.1) showed that the evolution of the $\varepsilon'_r = f(T)$ and $tg\delta = f(T)$ curves (Fig. 4) are closely related to the XRD patterns. Therefore we extensively pursued the synthesis of phase-pure perovskite and TTB phases. As mentioned above (cf. Section 3.2), the perovskite observed in the $K_2Sr_4(Mg_xNb_{10-x})Li_{3x}O_{30}$ compounds was synthesized as nearly pure for the $(K_{1/7}Sr_{4/7}Li_{1/7})(Mg_{1/7}Nb_{6/7})O_3$ composition. The corresponding dielectric curve (Fig. 11), after a 1200 °C for 2 h sintering, shows a very low dielectric constant (about 200). On the contrary, the nominal composition KSr_4MgNb_6, which is a mixture of TTB and perovskite phases, has an $\varepsilon'_r = f(T)$ curve with a higher dielectric constant, a maximum of ε'_r close to 1400 and a relatively flat temperature profile (Fig. 11).

At this stage, it appears that the high ε'_r constant and the presence of a maximum in the $\varepsilon'_r = f(T)$ curves of the $K_2Sr_4(Mg_xNb_{10-x})Li_{3x}O_{30}$ compounds, are related to the presence of the TTB phase, whereas the perovskite contributes only to a decrease of the average ε'_r constant of the mixture. In general, the compositions leading to a single, or a nearly single TTB phase show usually more attractive $\varepsilon'_r = f(T)$ curves.

3.7.1. Compositions with magnesium and full A-sites of the TTB structure

The $K_{2-3x}Sr_{4+3x}(Mg_xNb_{10-x})O_{30}$ compositions, with $x = 0.11$(D), $x = 0.13$(E), $x = 0.17$(F), $x = 0.22$(G) and $x = 0.33$(H) (Table III), which were sintered at 1300 °C for 10 h to achieve a relatively good densification, exhibit a dielectric constant higher than 1000 (Fig. 12). The maximum temperature decreases as x increases and is associated with a very broad

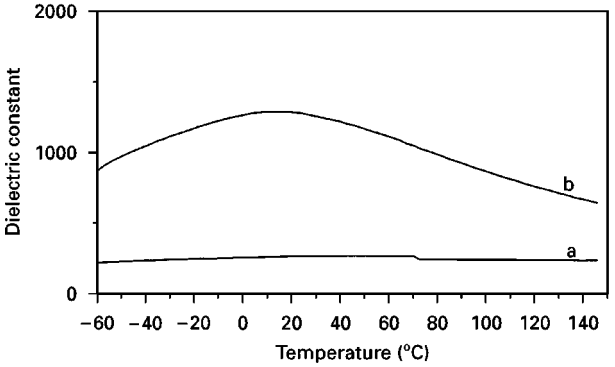

Figure 11 Dielectric constants versus temperature of samples, sintered at 1200 °C for 2 h and 1300 °C for 2 h, having the nominal compositions (a) $(K_{1/7}Sr_{4/7}Li_{1/7})$ $(Mg_{1/7}Nb_{6/7})O_3$ and (b) KSr_4MgNb_6, respectively.

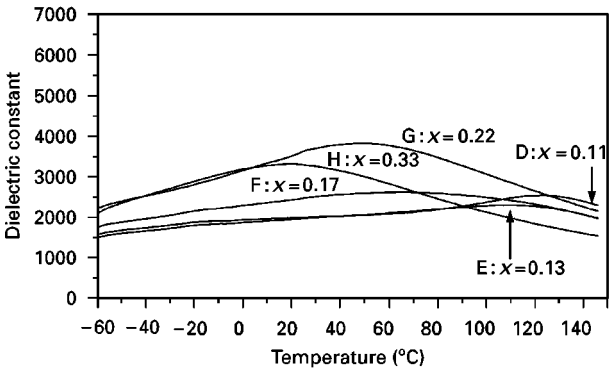

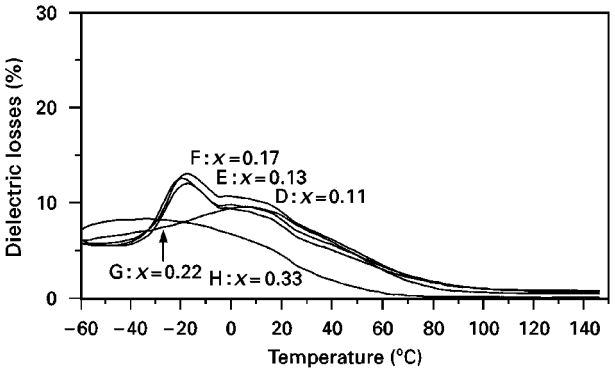

Figure 12 Dielectric constants and losses versus temperature of samples, sintered at 1300 °C for 2 h, having the compositions $K_{2-3x}Sr_{4+3x}(Mg_xNb_{10-x})O_{30}$ $(0.11 \leqslant x \leqslant 0.33)$.

maximum. In all cases, such trend could be interpreted by $Nb^{5+} - Mg^{2+}$ substitution, which is coupled to $K^+ - Sr^{2+}$ substitution, and would involve a larger disorder on the different sites of the TTB structure, concomitant with an increase in the distortion of the octahedra.

3.7.2. Compositions with lithium, but no magnesium and partially occupied A-sites of the TTB structure

The evolution of ε'_r versus temperature is quite different for the compositions J $(K_1Sr_{3.5}Nb_{10}Li_2O_{30})$ and K/$(K_{1.5}Sr_{3.5}Nb_{10}Li_{1.5}O_{30})$, which have an A-site cation-deficient TTB structure, with charge balance

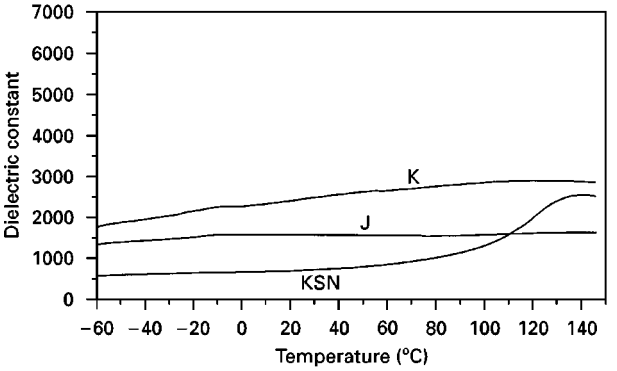

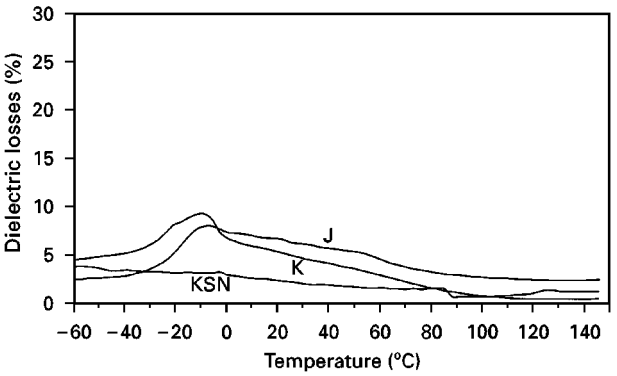

Figure 13 Dielectric constants and losses versus temperature of samples, sintered at 1200 °C for 2 h, having the nominal compositions $K_1Sr_{3.5}Nb_{10}O_{30}$ (J) and $K_{1.5}Sr_{3.5}Nb_{10}Li_{1.5}O_{30}$ (K) and, at 1300 °C for 2 h, for $K_2Sr_4Nb_{10}O_{30}$ (KSN).

obtained by incorporation of lithium in the structure. Fig. 13 compares the $\varepsilon'_r = f(T)$ curves of the J and K samples sintered at 1200 °C for 2 h to the $K_2Sr_4Nb_{10}O_{30}$ (KSN) one sintered at 1300 °C for 2 h (the presence of lithium allows good densification at lower temperature for samples J and K). In spite of relatively close compositions, the mean shape of the curves for J and K is quite different from that of KSN: the sharp maximum disappears leading to relatively flat curves. However, the mean dielectric constant remains lower than 3000. The broad maximum can be associated with both the distribution of K, Sr and Li elements and the vacancies in the tunnels of the TTB structure and the ability of lithium to occupy different sites. The existence of a compositional range for sample K certainly accentuates this phenomenon. In spite of the presence of lithium, one observes practically no increase of dielectric losses at high temperature for these compositions.

3.7.3. Compositions with lithium, magnesium and partially occupied A-sites of the TTB structure

The disorder on the A-sites of the TTB structure can be emphasized by coupling this to the substituion of Mg^{2+} for Nb^{5+} on the B-sites, as is the case for compositions A, B and C (Table III). The $\varepsilon'_r = f(T)$ and $tg\delta = f(T)$ curves (Fig. 14) should be compared with those given in Fig. 4 for the compositions $K_2Sr_4(Mg_xNb_{10-x})Li_{3x}O_{30}$.

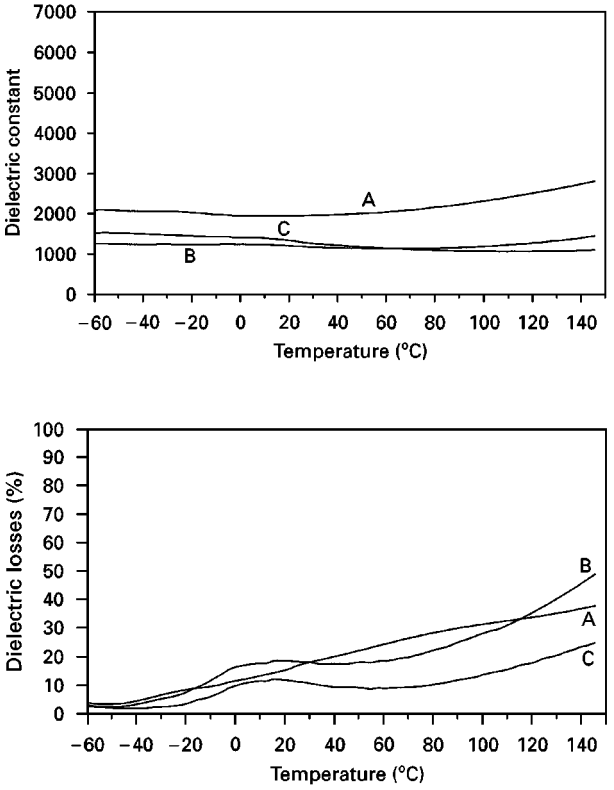

Figure 14 Dielectric constants and losses versus temperature of samples sintered at 1200 °C for 2 h, having the nominal compositions $K_{1.5}Sr_4(Mg_{0.5}Nb_{9.5})Li_2O_{30}$ (A), $K_{1.3}Sr_{3.7}(Mg_{0.4}Nb_{9.6})Li_{2.5}O_{30}$ (B) and $K_{1.3}Sr_{3.7}(Mg_{0.33}Nb_{9.67})Li_{2.29}O_{30}$ (C).

In fact, compositions A, B and C are situated in the compositional range deduced from the EDX analysis of the TTB phase of the $x = 0.67$ compound in Fig. 4. However, direct comparison of these two figures cannot be made, because, for the system reported in Fig. 4, the TTB coexists with a perovskite phase while in the other cases the TTB coexists with traces of the φ_i phases. For the A, B and C compounds, a small negative slope of the $\varepsilon'_r = f(T)$ curves is observed at low temperature, whereas an increase of ε'_r is observed at higher temperatures, which cannot distinctly be correlated with the drastic increase of dielectric losses, because of the different evolutions observed between the A, B and C curves. By comparing the two figures, Figs. 4 and 14, we can infer that the decrease of the maximum (of the ε'_r value), as observed in Fig. 4, seems to be more sensitive to the presence of lithium than to magnesium. This maximum is situated, for curves A, B and C, at a temperature lower than $-60\,^{\circ}C$, in spite of a decreased magnesium content. Since a nearly single-phase TTB is obtained for compounds A, B and C, a higher ε'_r level was expected for the materials whose curves are given in Fig. 14, i.e. samples where no low-dielectric-constant perovskite is present. The relatively low mean level of ε'_r can be due to either an increase in the lithium content, as already observed in Fig. 4, or to the presence of the secondary phases, φ_i, dispersed in the matrix. This observation lead us to investigate the influence of these secondary phases on the dielectric properties.

3.8. Influence of the secondary phases on the dielectric properties

Considering the samples which contain, after sintering, φ_1, φ_2 or φ_3 phases and their corresponding $\varepsilon'_r = f(T)$ and $tg\delta = f(T)$ curves, we can elucidate the influence of these phases on the dielectric properties. For samples with the TTB structure that also contain the φ_3 and φ_2 phases (A and B), a large increase of the dielectric losses is observed at high temperature. On the other hand, this effect is less significant for sample C, which contains both the φ_2 and φ_1 phases, and it disappears altogether for samples G and H, which contain only φ_1 phase as a secondary phase. Thus, high dielectric losses at high temperature appear to be correlated strongly to φ_3 and, to a lesser extent, to φ_2, but not to φ_1.

This conclusion is corroborated by the results observed for the nominal compositions $[(K_{1/7}Sr_{4/7}Li_{2/7})(Mg_{1/7}Nb_{6/7})]_{3/3.07}O_3$ and $Sr_6(Nb_8Mg_2)Li_4O_{30}$, where the φ_3 phase is present along with the main perovskite phase after sintering. An increase of the dielectric losses is indeed observed at high temperature for these compositions. Moreover for the $K_2Sr_4(Mg_xNb_{10-x})Li_{3x}O_{30}$ system $(0 \leqslant x \leqslant 1.33)$, the φ_3 phase only appears after sintering of samples having $x \geqslant 1$, and, for these values, similar evolution of both the $\varepsilon'_r = f(T)$ and $tg\delta = f(T)$ curves is observed (Fig. 4).

Owing to such trends of the $\varepsilon'_r = f(T)$ curves, when the φ_i phases are present, one can point out that these phases should exhibit very low dielectric constants and, thereby, induce a drastic decrease of the global dielectric constant of the corresponding ceramic.

4. Conclusions

In the compositions $K_2Sr_4(Mg_xNb_{10-x})Li_3O_{30}$, the contributions from two main phases, one with a TTB structure and the other with a perovskite-type structure, and those of minor phases, herein called φ_i, explain the evolution of the dielectric curves $\varepsilon'_r = f(T)$ and $tg\delta = f(T)$ as a function of nominal stoichiometry. The perovskite, whose composition was determined to be fixed as $(K_{0.14}Sr_{0.57}Li_{0.14})(Mg_{0.14}Nb_{0.86})O_3$, regardless of the nominal composition, exhibits a very low dielectric constant and consequently decreases the mean level of ε'_r of the mixture. In contrast, the TTB phase, whose ability to exhibit a range of cationic compositions was observed by electron diffraction coupled with EDX, strongly affects the profile of the $\varepsilon'_r = f(T)$ curves and tends to broaden the maximum with respect to temperature. The translation of maximum temperature toward low temperatures seems to be more sensitive to the presence of lithium than to the Nb–Mg substitution. Moreover, lithium promotes the formation of φ_i phases, which leads to high dielectric losses at high temperatures.

Through the various investigations aimed at synthesizing TTB and perovskite phases in pure forms, the Mg : Nb ratio on the octahedral sites was found to maximize for the TTB phase close to 0.05 : 1, whereas

for the perovskite phase it maximizes at 0.17:1. In both cases, cation deficiencies in the tunnels of the TTB and in A-sites of the perovskite were observed. In particular, different perovkite-type compounds, $(K_{0.14}Sr_{0.57}Li_{0.14})(Mg_{0.14}Nb_{0.86})O_3$, $(Sr_{0.65}Li_{0.15})(Mg_{0.15}Nb_{0.85})O_3$, $Sr_{0.8}(Mg_{0.2}Nb_{0.8})O_3$ and $Sr_{0.875}(Mg_{0.25}Nb_{0.75})O_3$, were synthesized, and a minimum A content of 0.8 was observed.

Concerning the dielectric properties, compositions with a TTB structure having cationic disorder on the different sites were shown to be interesting because their $\varepsilon'_r = f(T)$ curves exhibit a flat profile. Indeed, Nb–Mg mixing on the octahedral sites and, more importantly, K–Sr distributions on the A-sites, along with lithium and vacancies, strongly influence the dielectric curves. To clarify the effects of A-site distribution and to correlate the evolution of the TTB structure with the profile of its $\varepsilon'_r = f(T)$ curves, further studies in $K_2Sr_4Nb_{10}O_{30}$-based compositions without lithium are required and are currently being pursued.

Acknowledgements

Helpful comments from Dr. P. Salvador for the preparation of the manuscript are gratefully acknowledged.

References

1. B. BOUFROU, G. DESGARDIN and B. RAVEAU, *J. Amer. Ceram. Soc.* **74** (11) (1991) 2809.
2. J. M. HAUSSONNE, G. DESGARDIN, A. HERVE and B. BOUFROU, *J. Europ. Ceram. Soc.* **10** (1992) 437.
3. A. MAGNELI, *Arkiv. Chem.* **1** (1949) 213.
4. B. TRIBOTTE and G. DESGARDIN, *Mater. Sci. Eng.* **B40** (1996) 127.
5. B. A. SCOTT, E. A. GIESS, D. F. O'KANE and G. BURNS, *J. Amer. Ceram. Soc.* **53** (1970) 106.
6. F. GALASSO, in "Structure, Properties and Preparation of Perovskite-type Compounds" (Pergamon Press, New York, 1969).
7. B. TRIBOTTE and G. DESGARDIN, *J. de Phys. III France* **7** (1997) 1145.
8. J. RODRIGUEZ-CARJAVAL, in Satellite Meeting on Powder Diffraction Abstract on the XVth Conference of the International Union of Crystallography, Toulouse (1990) p. 127.
9. C. D. WHISTON and A. J. SMITH, *Acta. Crystallogr.* **23** (1967) 82.
10. F. GALASSO and J. PYLE, *J. Phys. Chem.* **67** (1963) 1561.
11. W. RIDGLEY, *J. Amer. Chem. Soc.* **77** (1955) 6132.
12. B. HESSEN, S. A. SUNSHINE, T. SIEGRIST and R. JIMENEZ, *Mater. Res. Bull.* **26** (1991) 85.
13. S. C. ABRAHAMS, P. B. JAMIESON and J. L. BERNSTEIN, *J. Chem. Phys.* **54–56** (1971) 2355.

Received 3 April
and accepted 23 June 1998